Chapter

ULF Geomagnetic Activity Signatures in the Atmospheric Parameters in Antarctica

Mauro Regi, Marcello De Lauretis, Gianluca Redaelli and Patrizia Francia

Abstract

The study of the solar wind-Earth's magnetosphere and atmosphere interaction is a topic of great interest. The solar wind energy is transferred to the Earth's environment also through ultralow frequency (ULF, 1 mHz–5 Hz) waves of the geomagnetic field, with higher efficiency at high latitudes where magnetic reconnection processes occur, making the polar cap an important laboratory for these investigations. Several studies suggest that the atmosphere responds to the geomagnetic activity driven by the solar wind, although the interaction processes are not yet completely understood. In this context, the results of recent investigations, showing the coupling on timescales of 1–2 days between geomagnetic ULF activity and the middle-low (h < 50 km) atmosphere in the polar cap, are summarized, based on geomagnetic measurements at Terra Nova Bay, in Antarctica ($\lambda \sim 80°S$) and atmospheric parameters from the reanalysis dataset.

Keywords: ULF waves, solar wind, high-latitude atmosphere, polar cap electrodynamics, energetic particle precipitation, atmosphere processes, cloud microphysics

1. Introduction

In the latest years, the Sun-Earth environment is studied to explain observed physical phenomena in the context of space weather/climate, such as climate changes. It is well known that the Sun continuously transfers its energy to the Earth's environment through radiation and solar wind (SW). Although the Sun's radiation represents the main source affecting the Earth's atmosphere, the SW energy plays an important role during high geomagnetic activity time intervals [1]. On this regard, the magnetosphere-ionosphere represents a complex system able to partially convert SW impacting energy through nonlinearly related physical processes. Such effects are more evident at high latitudes where reconnection processes between interplanetary magnetic field (IMF), carried out by the solar wind, and magnetospheric field occur, making the polar cap an important laboratory to study the SW-atmosphere interactions. Solar wind-driven electrodynamic processes and ultralow frequency (ULF, 1 mHz–5 Hz) waves seem to lead to both diffusion and precipitation processes of energetic electrons in the outer radiation belts, leading

also to chemical [2] and microphysical [3] processes in the atmosphere, characterized by different timescales.

The longer-term response, characterized by timescales of several weeks, is usually attributed to the odd nitrogen (NOx) production, due to precipitating energetic electrons, in the mesosphere and lower thermosphere. During the polar winter, NOx can live long enough to be transported downward into the stratosphere where it chemically perturbs the ozone distribution, altering the radiative balance in that region of the atmosphere.

This can in turn affect the overall circulation in the stratosphere, and such changes can propagate to the surface level, eventually leading to detectable changes in surface air temperatures, through dynamical coupling processes occurring on timescales of several weeks (e.g., [2, 4–6]).

Conversely, the shorter-time response (<1 day) of the atmosphere to the SW-magnetosphere coupling processes is probably related to changes in the atmospheric electrodynamics. It can be attributed to electric conductivity variations in the lower atmosphere by ionization mechanisms and/or to changes of the polar cap electric potential induced by SW perturbations [7]. The consequent modulation of the current density which flows from the upper boundary (being as low as 60 km, [8]) through the troposphere to the ground in the global electric circuit (GEC) [3, 9–11] could influence cloud formation through the release of latent heat, which in turn can affect atmospheric dynamics [12].

This work represents a review of our investigations on the experimental observation of the possible short (within ~1 day) timescale response of the atmosphere to the SW dynamics, observed during 2003–2010, which correspond to the solar cycle 23 and the beginning of solar cycle 24. We analyzed the geomagnetic field variations monitored at the Mario Zucchelli station, at Terra Nova Bay (TNB, AACGM latitude λ = 80.01°S and longitude φ = 306.94°E) in Antarctica, and atmospheric parameters at tropospheric and stratospheric heights, provided by ERA-Interim and Monitoring Atmospheric Composition and Climate (MACC) reanalysis archives (http://apps.ecmwf.int/datasets).

The ERA-Interim is a global atmospheric reanalysis dataset, continuously updated in real time (see [13] and references therein). Global atmospheric and surface parameters from 1 January 1979 are available from the surface up to 0.1 hPa as atmospheric fields on model levels and pressure levels, with a temporal resolution of 6 h, and as surface fields with a temporal resolution of 3 h. The data assimilation system used to produce ERA-Interim is based on a 2006 release of the ECMWF Integrated Forecast Model (IFS Cy31r2). The MACC dataset is a global reanalysis dataset of atmospheric composition data, produced by assimilating satellite data into a global model and data assimilation system (see [14] and references therein). The system includes a four-dimensional variational analysis (4D-Var) with a temporal resolution of 12 h analysis window. The ERA-Interim and MACC data, at 1 day resolution used for our studies, have been retrieved from the Meteorological Archival and Retrieval System at ECMWF.

Solar wind parameters and interplanetary magnetic field are monitored by using OMNI data, time-shifted to the bow shock nose (i.e., the subsolar position of the supersonic-to-subsonic transition regions) and collected on CDAWeb (http://cdaweb.gsfc.nasa.gov). Geomagnetic activity was monitored by using a triaxial search-coil magnetometer data, recorded at TNB, at a sampling rate of 1 s.

The atmospheric parameters must be whitened to filter the longer period components (essentially 1 year and 6 months), which would obscure the weak effects produced by the ULF geomagnetic activity [15].

This review is structured as follows: in Section 2, we shortly introduce the interactions occurring between ULF waves and the energetic electrons in the outer

radiation belt, leading particle precipitations, as well as polar cap potential difference related with SW parameters; in Section 3, we present the experimental evidence of SW effects on the atmospheric parameters in Antarctica at stratospheric and tropospheric heights; finally, in Section 4, we discuss the estimated timescale response of atmospheric parameters and the possible physical processes involved in SW-atmosphere coupling processes. For greater clarity, we described data analysis and methods in each section.

2. The solar wind-magnetosphere coupling processes at high latitudes

The estimation of the Earth's surface temperature and lower atmosphere energy budget significantly changes due to small amount, distribution, or radiative properties of clouds [16]: therefore, they represent one of the largest sources of uncertainty in predictions of climate change [17]. Even small atmospheric electrical modulations can affect aerosol nucleation processes and cloud condensation nuclei production in troposphere and thus modify cloud properties. In this regard, the polar cap electrodynamics and the energetic particle precipitation seem to be important SW-atmosphere coupling mechanisms, responsible for atmospheric changes on timescales from several weeks to days. It is also known that a global electric current flows in the global electric circuit. It is generated mainly by charge separation in clouds at the tropics and maintains the global ionosphere at a potential of about 250 kV. Variations above and below this value occur in the high-latitude regions due to SW-magnetosphere-ionosphere coupling processes. In this section, we briefly discuss the solar wind-magnetosphere coupling processes, which could produce observable effects in the stratospheric and tropospheric dynamics due to energetic particle precipitation from the outer radiation belt, as well as to the polar cap electrodynamics at high latitudes.

2.1 ULF interaction with relativistic electrons in the outer radiation belts

ULF magnetohydrodynamic waves received particular attention in the past decades [18–23], since they provide a convenient probe of the magnetosphere, by means of ground [24–26] and/or satellites magnetic field measurements [22, 27–30] as well as inspect ground conductivity [31–33].

Generated by a variety of instabilities, ULF waves transport energy throughout the magnetosphere and are observed on the ground as continuous pulsations (Pc, **Table 1**). They can play important roles in the energization and loss of radiation belt particles (see [34] for a review). In particular, ULF waves can interact with the relativistic electrons (>300 keV) magnetically trapped in the radiation belts ($L \sim 5$–7 Re, $\lambda \sim 60$–$70°$, where L is the McIlwain parameter). In that regions, the charged particle is subject to gyro, bounce, and drift periodic motions (see **Table 1**), each one characterized by different timescales [35–36].

In particular, wave-particle interactions are theoretically predicted [37, 38] because drift and bounce motion frequencies of trapped electrons are in the Pc5 (1–7 mHz) and Pc1-2 (100 mHz–5 Hz) frequency range, respectively. Experimental evidence confirms diffusion/acceleration of energetic electrons by Pc5 magnetospheric waves [39–42] and their precipitations after pitch angle scattering, due to gyro-resonant interaction with electromagnetic ion cyclotron (EMIC) waves [38–41]. Such waves are in the Pc1-2 frequency range and are generated at the magnetic equator by unstable distributions of ring current ions during geomagnetic storms [43]. Moreover, recent investigations show that Pc5 waves have their origin also in the leading edge of the corotating interaction regions (CIR) [42], while the

ULF waves			Magnetically trapped particles		
Pulsation type	Frequency range (mHz)	Period range (s)	Characteristic periodicity (s)		Motion type
			Electrons	Protons	
Pc5	2–7	**150–600**	**10^2–10^3**	10^2	**Drift**
Pc4	7–22	45–150	—	—	—
Pc3	22–100	10–45	—	—	—
Pc2	100–200	5–10	—	—	—
Pc1	200–5000	**0.2–5**	**10^{-1}**	10^0	**Bounce**
—	—	—	10^{-3}–10^{-4}	10^{-1}–10^{-2}	Gyro

Periodicity correspondence between relativistic electrons and ULF waves is marked in bold.

Table 1.
ULF wave classification and the characteristic timescales for the three types of trapped particle motion (see also [37]).

origin of the Pc1-2 waves, observed at ∼80° latitude, appears to be due to substorm/storm-related instabilities and, in the dayside, to solar wind compressions of the magnetopause [44]. After conversion into Alfvén (shear) waves, ULF waves propagate along the geomagnetic field lines and can be observed on the ground at high latitudes [45, 46]. An example of energetic electron flux enhancements observed at geosynchronous orbit ($L \sim 6.6$) associated to Pc5 power fluctuations measured on the ground and in the magnetosphere is shown in **Figure 1**, [42]; the electron flux seems to be delayed by ∼2 days with respect to pulsation power.

2.2 The roles of relativistic electron precipitation and the polar cap electrodynamics in the global electric circuit model at high latitudes

As discussed by Tinsley and Yu [48], the galactic cosmic rays (GCR) flux is responsible for almost all the production of ionization below 15 km of altitude, which determines the conductivity in that region and at high latitudes. However, the MeV electrons and their associated X-rays produce ionization in the stratosphere and higher troposphere, which can affect the local conductivity (see also [7]). Moreover, due to electric potential difference between the ionospheric layer and the ground, a vertical current density is present:

$$J_z = \sigma E_z. \tag{1}$$

It is directed along the stratosphere-troposphere-ground direction z, and it varies horizontally, due to variations in the local vertical column resistance represented by its resistivity σ and by variations in the local ionospheric potential $\varphi(\mathbf{E})$. While σ is affected by the GCR and precipitating MeV electron fluxes from the outer radiation belt into the atmosphere, $\varphi(\mathbf{E})$ is strongly dependent on SW-magnetosphere coupling process. In particular, the potential increases in the polar cap where geomagnetic field lines map to magnetospheric regions characterized by coupling processes with the interplanetary magnetic field (IMF); because J_z, flowing through clouds in the troposphere, responds to conductivity and potential changes occurring up to 120 km altitude, it is very effective in linking stratosphere and ionosphere with clouds. Recent reviews by Lam and Tinsley [3] and Mironova et al. [7] well discuss the atmosphere response to current density changes near the poles caused by the interaction of the solar wind with the geomagnetic field; such

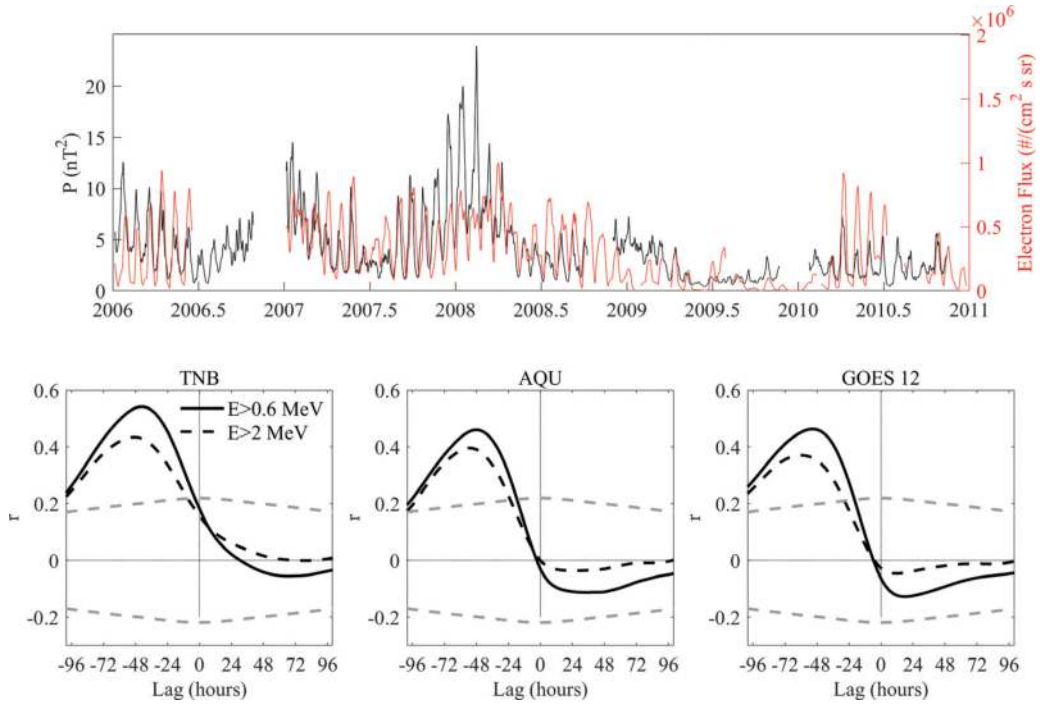

Figure 1.
(Top) The relativistic electron flux (>600 keV) measured by GOES 12 satellite at geosynchronous orbit (red) and the geomagnetic power at TNB (black). (Bottom) The cross-correlation of the >600 keV (solid) and >2 MeV (dashed) electron flux with the Pc5 power at TNB, at low latitude station of L'Aquila AQU, and at GOES 12 during 2007–2008, together with the 95% confidence levels (dashed, gray lines). Figure adapted from [42]. It clearly emerges a higher correlation with the >600 keV electron flux at a shorter-time delay (1.8–2 days) with respect to the >2 MeV electrons (2–2.4 days), with an approximately 9 h difference, probably due to the timescales of the acceleration processes, in agreements with [47].

changes arise in addition to the day-to-day variability in J_z, caused by thunderstorm activity and present at all latitudes.

In particular, the B_y (dawn-dusk) and B_z (south-north) components of the IMF represent the main parameters controlling the electrodynamics in the upper atmosphere (i.e., the ionosphere): B_z is important in the reconnection process in the dayside magnetopause, while B_y affects the latitudinal dawn-dusk electrostatic potential asymmetry [49].

An example of polar cap electric potential in the southern hemisphere is show in **Figure 2**, obtained using the Weimer [50, 51] ionospheric electrodynamic model. In this example, we assigned values of ± 5 nT for B_y and B_z, assuming a solar wind speed of V_{SW} = 450 km/s and a solar wind number density of n_{SW} = 3 cm^{-3}. It is clearly seen that two regions of polar cap potential, characterized by positive (dawnward) and negative (duskward) values of approximately ± 40 kV, are emerging during periods characterized by SW-magnetosphere coupling (i.e., during $B_z < 0$), indicating higher dawn-dusk polar cap potential drop. Conversely, during closed magnetosphere ($B_z > 0$, left panels), lower polar cap potential difference is obtained. It implies that E_z increases at high latitudes during IMF-magnetosphere reconnection ($B_z < 0$) conditions. Furthermore, both σ and E_Z in Eq. (1) can be significantly influenced by geomagnetic activity. In this regard, ULF activity could play an important role in the GEC model, leading to the clouds' physical changes and radiative properties. Indeed, the ULF activity in general is associated to storms and substorms, i.e., to the occurrence of a southward IMF and, at high latitudes, polar cap electric field; therefore, ULF activity can be regarded also as a proxy of the polar cap potential difference [52, 53].

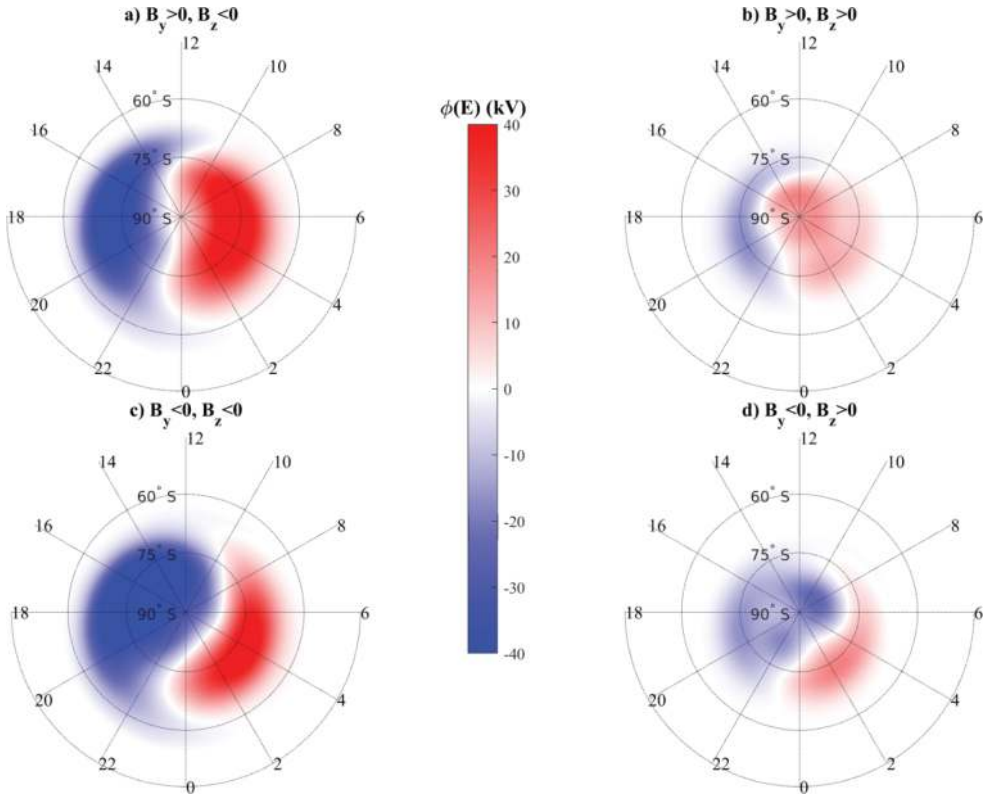

Figure 2.
Computed polar cap electric potential, obtained using Weimer [50, 51] ionospheric electrodynamic model at the equinoctial day 100 of the year 2000 in the southern hemisphere, for open (B_z < 0, left panels) and closed (B_z > 0, right panels) magnetospheric conditions. The meridians are separated by 2 h (MLT) and the geomagnetic parallels by 15°. The morning (afternoon) side corresponds to the right (left) side of each panel.

3. Experimental evidence of signatures of solar wind effects in the atmospheric parameters

In their study, Francia et al. [15] examined surface air temperature measured at the automatic weather station ENEIDE, located at TNB, during 2007–2008, while signatures of ULF activity and polar cap potential difference were found by [54] in the stratosphere and troposphere, using the ERA-Interim reanalysis dataset.

Figure 3 shows the global wavelet (GW), i.e., the time-averaged wavelet [55, 56], separately for summer and winter months, of Pc5 and Pc1-2 powers at TNB and of the polar cap potential difference φ_{cap} [54].

Common power peaks emerge at ~27 days, the Sun synodic rotation period, and its first subharmonics (13.5 and 9 days), in the SW-related parameter φ_{cap} and correspondingly in the ULF activity. In particular, in **Figure 4** signatures of ULF activity and polar cap potential difference in temperature T and zonal wind U at tropospheric and stratospheric heights above TNB are observed. In their work [54], cross-wavelet W_{xy} and wavelet coherence γ^2 [56] are computed between SW-driven and atmospheric parameters; the analysis was supported by the Monte Carlo test for the estimation of significance levels.

In can be seen from **Figure 4** that the correspondence at 27 days is high and statistically significant in both the troposphere and the stratosphere during winter months, while at 13.5 days it is restricted to h < 10 km. During summer, the cross-wavelet W_{xy} for T shows very low values and an ambiguous correspondence at the

DOI: http://dx.doi.org/10.5772/intechopen.81106

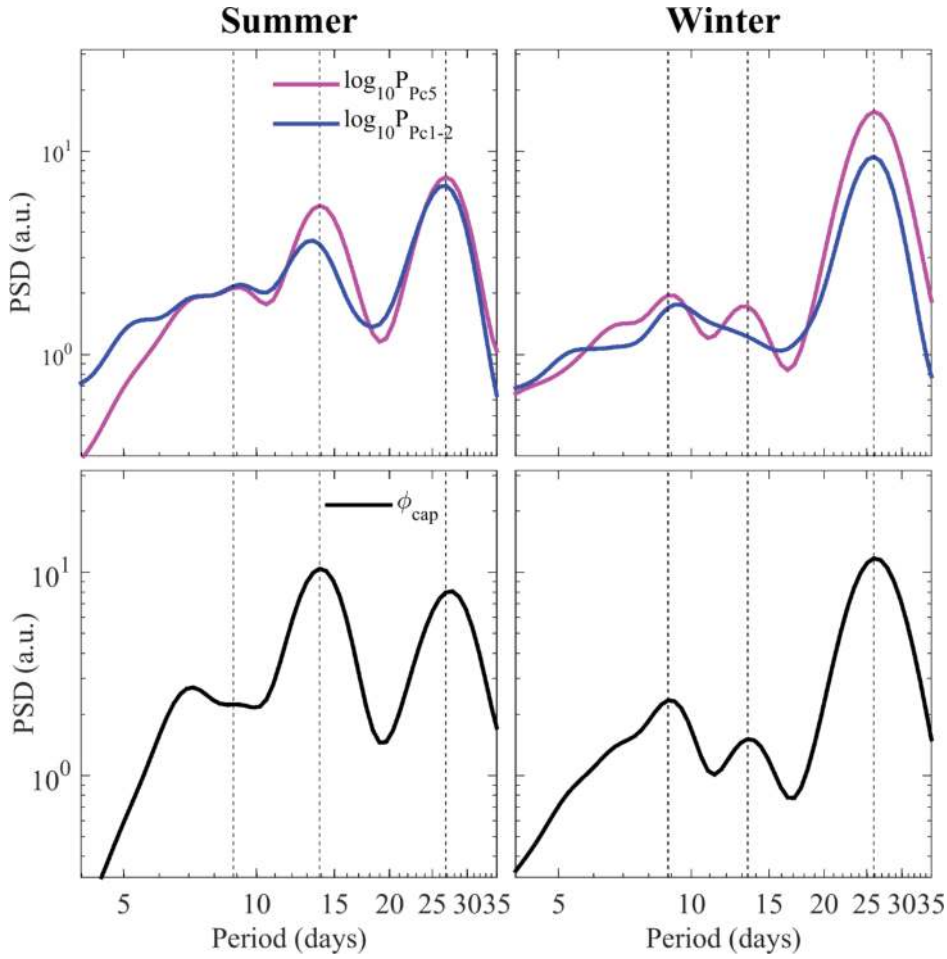

Figure 3.
The normalized global wavelet (GW) analysis during the summer (first column) and winter (second column) in 2007 (top panels); the GW, normalized to the corresponding variances, of the ULF activity indexes logPc5 and logPc1-2 at TNB, and of φ_{cap} *(bottom panels). The three first maximum values of the normalized GW are marked with vertical lines. Figure adapted from [54].*

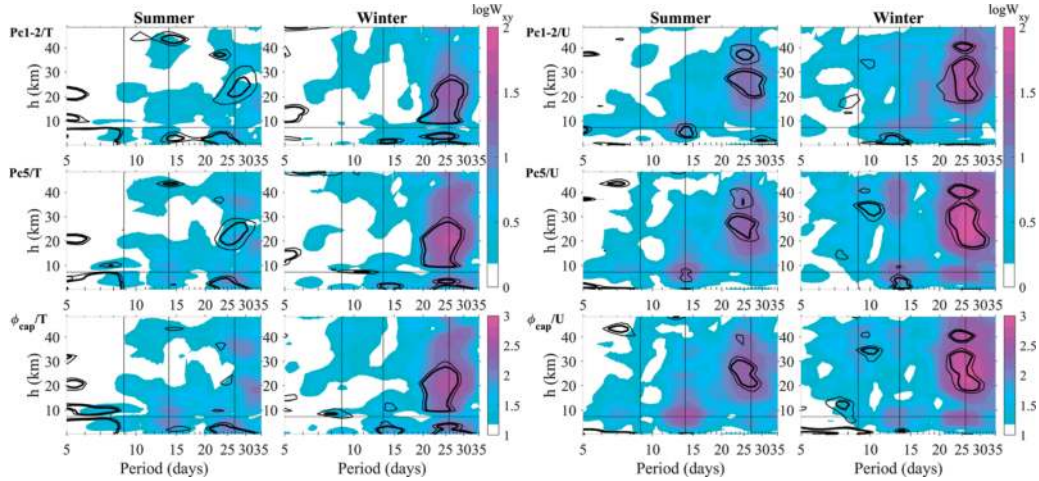

Figure 4.
Time averaged cross-wavelet amplitude (W_{xy}) *between temperature* T *and zonal wind* U *with (top) logPc1-2, (middle) logPc5, and (bottom) polar cap potential difference* φ_{cap} *during summer and winter months in 2007, as a function of period and altitude* h*. In each panel, the black contour lines mark the 90% (thin) and 95% (bold) significance level of time-averaged wavelet coherence. Vertical lines indicate the periodicities observed in solar wind and geomagnetic activity (**Figure 3**). Figure adapted from [54].*

27 day periodicity for all input parameters. Interestingly, a W_{xy} and γ^2 attenuation can be seen, especially during winter months, near to the tropopause position (~7–10 km). Regarding U, high and significant W_{xy} and γ^2 values are found mostly in the stratosphere, at ~27 and ~13.5 day periodicities, during winter months. During summer the pattern is similar but with lower values.

Analyzing the tropospheric temperature, specific humidity Q and cloud cover (CC) in Antarctica, Regi et al. [57] found further experimental evidence of SW-atmosphere coupling. In particular, the authors analyzed 54 high geomagnetic activity time intervals, by using the superposed epoch analysis with the Monte Carlo test [58].

The results, shown in **Figure 5**, revealed a clear correspondence between Pc1-2 and variations in temperature, specific humidity, and cloud cover. The most significant correspondence is found at latitudes higher than 85°S in both T and Q parameters. Positive variations occurred at the epoch and 1 day after, suggesting that Pc1-2 power affects the specific humidity and the tropospheric temperature within 1 day; negative variations occurred at 2 days after the epoch.

Regarding the cloud cover (zonal mean) composite averages, computed at low (LCC, $h < 3$ km), medium (MCC, $3 < h < 6$ km), and high (HCC, $h > 6$ km) altitudes, (see **Figure 5**, bottom panels), we found that the main effect of the ULF activity on these parameters consists in an increase in the HCC and MCC at the epoch. Moreover, we also found a significant variation at 1 day after and a decrease at 2 days after the epoch.

As discussed in the Introduction, GEC affects atmospheric parameters, such as cloud cover through several proposed microphysical processes (e.g., [3, 10, 48])

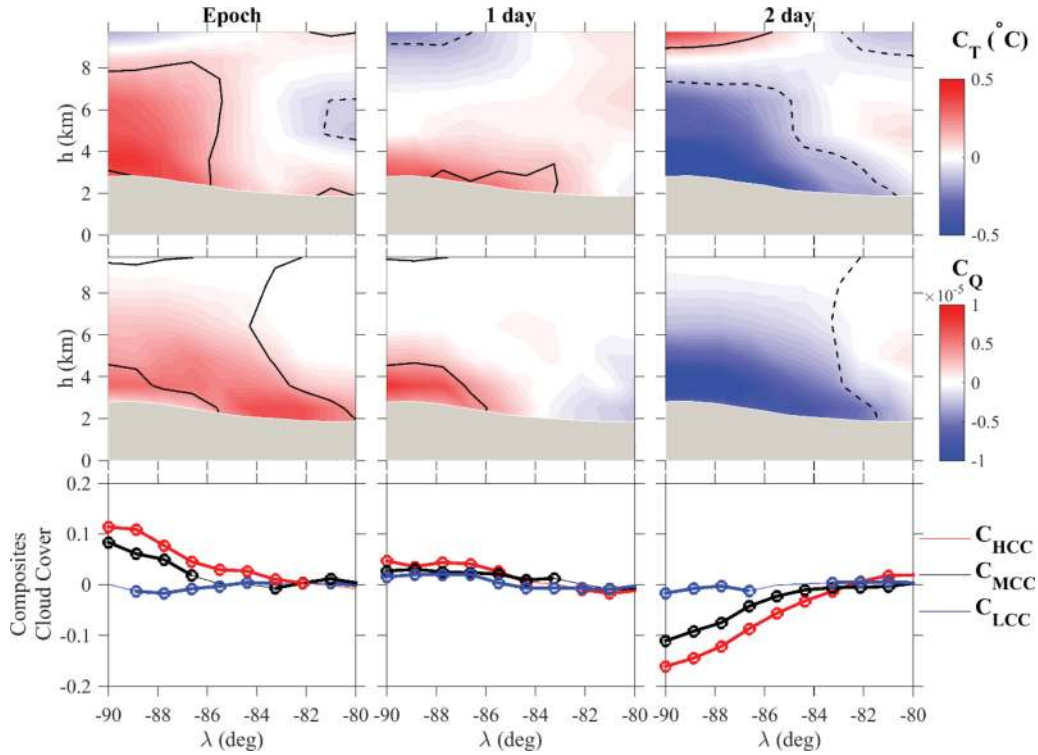

Figure 5.
(Top and middle panels) Composites of the zonal mean of temperature C_T and specific humidity C_Q of 54 selected epochs (corresponding to geomagnetic active periods) as a function of latitude and altitude. Solid and dashed lines indicate the 90% confidence levels. The gray region represents the longitudinally averaged Antarctic icy surface profile. (Bottom panels) Composite mean of cloud cover at different altitudes C_{LCC} (h < 3 km), C_{MCC} (3 < h < 6 km), and C_{HCC} (h > 6 km) as a function of latitude; the bold lines mark composites statistically relevant. Figure adapted from [57].

able to produce changes in the atmospheric parameters, such as temperature. In particular, the accumulation of charge on droplets and aerosol particles, most importantly the interstitial cloud condensation nuclei (CCN) and ice-forming nuclei (IFN), directly affects scavenging rates.

Scavenging is due to collisions between the nuclei and droplets, entailing size-dependent collection of nuclei and changes in their size distribution and overall concentration. It affects a number of microphysical processes, which cause changes in macroscopic cloud properties and in turn partitioning of energy flow in the system. In particular, the charge can increase or decrease the scavenging rates, depending on size, changing the concentrations and size distributions. Size distribution changes in CCN produce size distribution changes in droplets, affecting coagulation, precipitation, latent heat transfer, and cloud cover. Scavenging of ice-forming nuclei by supercooled droplets promotes contact ice nucleation, releasing latent heat. The latent heat changes cause storm invigoration [59] and in winter storms can cause changes in the amplitude of Rossby waves and blocking. Since the typical lifetime of CCN in an air mass can be up to 10 days, the change in their properties can affect also later cycle of evaporation/condensation, flux of latent heat, and the amount of water vapor released into the troposphere.

Figure 6 shows the results of superposed epoch analysis (SEA) conducted by [57] on Q and T at the epoch for different orientations of the IMF. It shows correspondence in T and Q, more evident during the IMF $B_z < 0$ and $B_y > 0$ conditions, i.e., when the interplanetary electric field is efficiently transmitted into the high-latitude ionosphere and the dawn-dusk polar cap potential difference φ_{cap}, due to $E_y = -V_{SW}B_z$, as well as the vertical $E_z = V_{SW}B_y$, increases (see also **Figure 2**). In particular, the vertical electric field during southward IMF conditions can be directly transferred in the ionospheric polar cap in the southern hemisphere,

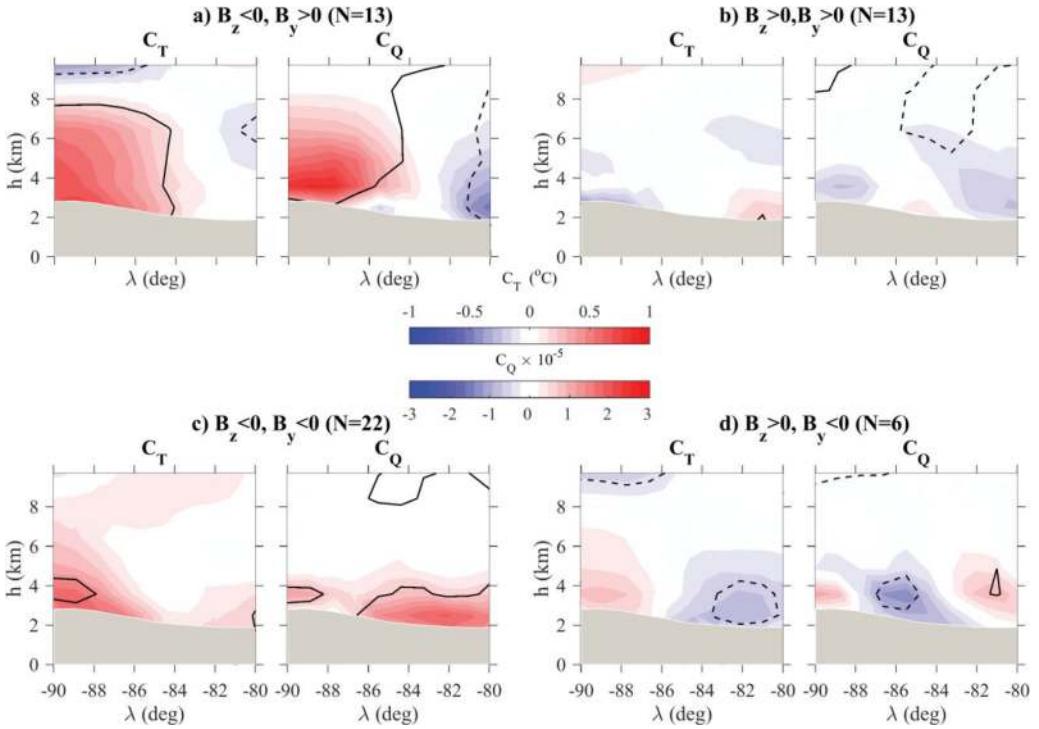

Figure 6.
Composites of the zonal mean of temperature C_T and specific humidity C_Q at the epoch for different orientations of the IMF, where N *represents the number of cases. Solid and dashed lines indicate the 90% confidence levels. The gray region represents the longitudinally averaged Antarctic icy surface profile. Figure adapted from [57].*

leading to a vertical current $J_z = \sigma E_z$ from the ionosphere to the ground through the stratospheric and tropospheric layers.

4. The observed timescales of the response of the atmosphere to SW variations

Timescales are important in order to discriminate the involved physical processes in the SW-atmosphere coupling. In their pioneering work, Francia et al. [15] found that, during 2007 and 2008, the ULF activity, in both Pc1-2 and Pc5 frequency ranges, is correlated with the surface air temperature with different delays. Their results, shown in **Figure 7a**, indicate that the temperature is significantly correlated with the Pc1-2 power at a time lag of 1 day. Although lower, the correlation with the Pc5 power is also significant, reaching the maximum value when the temperature is delayed by 3 days with respect to the Pc5 power.

In the meanwhile, Regi et al. [57] computed the cross-correlation between high cloud cover (HCC, h > 6 km) over Antarctica and logPc1-2 time series at TNB during 2003–2010, band-pass filtered at ~27 days. They found several Antarctic regions characterized by significantly high correlation values. Examples of positive cross-correlations are shown in **Figure 7b**. Their experimental results suggest an average time delay of approximately 1 day of the response of the atmospheric cloud cover to the SW-driven Pc1-2 ULF power intensification. Such delay is consistent with the timescales of electrodynamics−/microphysical-related processes here proposed. In [57] a possible relationship with large-scale atmospheric transport was investigated by means of a correlation analysis between Pc1-2 power and CH_4 (~27 day band-pass filtered) concentrations from MACC dataset. CH_4 is a long life chemical tracer, commonly used to characterize the middle atmosphere transport, also analyzing it in the framework of quasi-Lagrangian or conservative coordinate systems [60] and as a proxy to validate satellite measurements [61]. The results of the correlation analysis between Pc1-2 power and CH_4, during 2003–2010 (not shown here), indicate that the correlation coefficients are generally lower and not significant and superimposable to the other tropospheric parameters. They suggest that the transport is not modulated by the 27 day periodicity of the ULF activity.

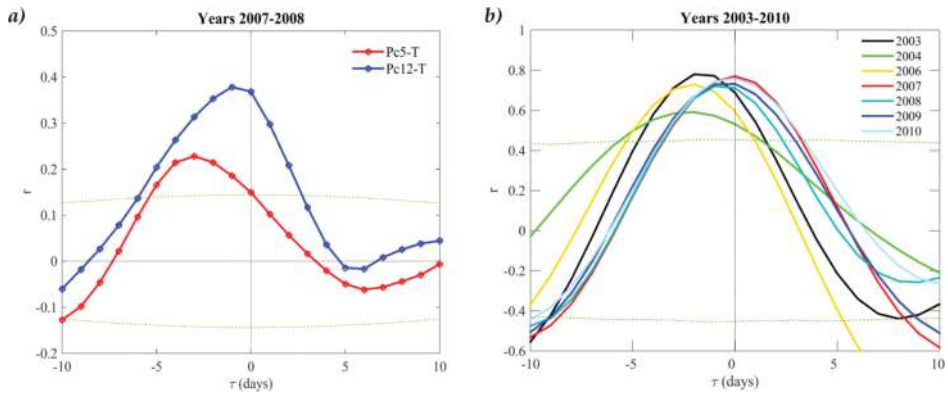

Figure 7.
(a) The cross-correlation between the Pc5 and the Pc1-2 power and the surface air temperature, at TNB, at different time lags τ. A delay τ < 0 (τ > 0) indicates that Pc1-2/Pc5 power precedes (follows) surface air temperature at TNB. The dashed green lines represent the 90% confidence level. Figure adapted from [15]. (b) Examples of positive cross-correlation analysis as a function of the delay of the HCC with respect to Pc1-2 power, observed during winter months of 2003–2010. The green lines mark the 95% confidence level. A delay τ < 0 (τ > 0) indicates that Pc1-2 power precedes (follows) HCC. Figure adapted from [57].

However, the different time delays in different years could be due to variations in large-scale transport pattern (see [57] for details).

5. Summary and conclusions

In this work we presented a short review of our experimental results regarding the possible relationship between SW and atmospheric parameters at high latitude, in Antarctica, at Terra Nova Bay. Examining possible relationship between geomagnetic activity in the Pc1-2 and Pc5 frequency range and the polar cap potential difference with stratospheric and tropospheric parameters, the results provided in [54] can be summarized as follows:

- Common power peaks emerge at ∼27 days, the synodic Sun rotation period, and its first subharmonics (13.5 and 9 days), in the polar cap potential difference φ_{cap} and in the ULF activity (**Figure 3**) and in the temperature and zonal wind at tropospheric and stratospheric altitudes (**Figure 4**).

- The correspondence is more evident during winter, when solar radiation-driven processes are absent.

- Around the tropopause, approximately at 8 km, the correspondence is low, and in the stratosphere it appears mostly at the 27 day periodicity.

Further investigations [57] at tropospheric heights at high latitudes indicate that SW-driven electrodynamic processes and energetic particle precipitation related with enhancement of Pc1-2 activity can affect tropospheric temperature, specific humidity, and cloud cover. The response is quick (within ∼1 day) at ground and in the troposphere. These results suggest that the electrodynamics modulate the physical properties of clouds, probably through electron scavenging microphysical mechanism. It is a matter of fact that electron scavenging is strongly dependent on vertical tropospheric-stratospheric conductivity variations, due to energetic particle precipitation driven by ULF waves, and on the vertical electric current, modulated by polar cap potential, associated to SW-magnetosphere reconnection processes. More recently, evidence of an SW signature in the mesosphere [62] has been published, indicating that the SW can affect the atmosphere through the whole atmospheric column. As discussed by [63], the processes involved in each atmospheric layer are almost certainly different, and transport phenomena could be important.

Our conclusions are supported by the observed short (<1–2 days) delay response in the atmospheric parameters at troposphere altitudes and at ground with respect to the much longer delay expected for chemical mechanism [15, 57]. However, this matter should be further investigated as underlined by [63] in particular through the examination of the time delays at stratospheric and mesospheric altitudes and at lower latitudes; the study of the dependence on different interplanetary conditions might be also useful for a more deep understanding of the atmosphere response to the SW.

Acknowledgements

The authors acknowledge J. H. King and N. Papatashvilli at NASA and CDAWeb for solar wind data (http://cdaweb.gsfc.nasa.gov) and Daniel Weimer at Space

Science Center for Space Science and Engineering Research (Virginia Tech) who provided the ionospheric electrodynamic model. The authors would also like to thank the MACC and ERA-Interim project data provider. The reanalysis data were provided by the European Centre for Medium-Range Weather Forecasts (ECMWF) and can be downloaded from the ECMWF Data Server (http://apps.ecmwf.int/datasets). Measurements of the geomagnetic field fluctuations at Terra Nova Bay are supported by the Italian PNRA (Programma Nazionale di Ricerche in Antartide, PdR2013/B2.09).

Conflict of interest

The authors declare that they are not competing interests.

Author details

Mauro Regi[1*], Marcello De Lauretis[1], Gianluca Redaelli[2] and Patrizia Francia[1]

1 Department of Physical and Chemical Sciences, University of L'Aquila, L'Aquila, Italy

2 CETEMPS, Department of Physical and Chemical Sciences, University of L'Aquila, L'Aquila, Italy

*Address all correspondence to: mauro.regi@aquila.infn.it

References

[1] de Wit TD, Watermann J. Solar forcing of the terrestrial atmosphere. Comptes Rendus Geoscience. 2010; **342**(4–5):259-272

[2] Seppälä A, Lu H, Clilverd MA, Rodger CJ. Geomagnetic activity signatures in wintertime stratosphere wind, temperature, and wave response. Journal of Geophysical Research: Atmospheres. 2013;**118**(5):2169-2183

[3] Lam MM, Tinsley BA. Solar wind-atmospheric electricity-cloud microphysics connections to weather and climate. Journal of Atmospheric and Solar-Terrestrial Physics. 2016;**149**: 277-290

[4] Rozanov E, Callis L, Schlesinger M, Yang F, Andronova N, Zubov V. Atmospheric response to NOy source due to energetic electron precipitation. Geophysical Research Letters. 2005; **32**(14):L14811

[5] Lu H, Clilverd MA, Seppälä A, Hood LL. Geomagnetic perturbations on stratospheric circulation in late winter and spring. Journal of Geophysical Research. 2008;**113**(D16):D16106

[6] Baumgaertner AJ, Seppälä A, Jöckel P, Clilverd MA. Geomagnetic activity related NO x enhancements and polar surface air temperature variability in a chemistry climate model: Modulation of the NAM index. Atmospheric Chemistry and Physics. 2011;**11**(9): 4521-4531

[7] Mironova IA, Aplin KL, Arnold F, et al. Energetic particle influence on the Earth's atmosphere. Space Science Reviews. 2015;**194**(1–4):1-96

[8] Tinsley B. The global atmospheric electric circuit and its effects on cloud microphysics. Reports on Progress in Physics. 2008;**71**(6):66801

[9] Tinsley BA, Zhou L. Initial results of a global circuit model with variable stratospheric and tropospheric aerosols. Journal of Geophysical Research. 2006; **111**(D16):D16205

[10] Tinsley BA, Burns GB, Zhou L. The role of the global electric circuit in solar and internal forcing of clouds and climate. Advances in Space Research. 2007;**40**(7):1126-1139

[11] Rycroft MJ, Nicoll KA, Aplin KL, Harrison RG. Recent advances in global electric circuit coupling between the space environment and the troposphere. Journal of Atmospheric and Solar-Terrestrial Physics. 2012;**90**:198-211

[12] Markson R. Modulation of the Earth's electric field by cosmic radiation. Nature. 1981;**291**(5813):304

[13] Simmons A. ERA-interim: New ECMWF reanalysis products from 1989 onwards. ECMWF Newsletter. 2006; **110**:25-36

[14] Inness A, Baier F, Benedetti A, et al. The MACC reanalysis: An 8 year data set of atmospheric composition. Atmospheric Chemistry and Physics. 2013;**13**:4073-4109

[15] Francia P, Regi M, De Lauretis M. Signatures of the ULF geomagnetic activity in the surface air temperature in Antarctica. Journal of Geophysical Research: Space Physics. 2015;**120**(4): 2452-2459

[16] Hartmann DL. Chapter 6-Radiative effects of clouds on earth's climate. In: Hobbs PV, editor. Aerosol-Cloud-Climate Interactions. International Geophysics. Academic Press; 1993;**54**: 151-173

[17] Intergovernmental Panel on Climate Change, editor. Climate Change

2013—The Physical Science Basis: Working Group I Contribution to the Fifth Assessment Report of the Intergovernmental Panel on Climate Change. Cambridge: Cambridge University Press; 2014

[18] Eriksson PTI, Blomberg LG, Schaefer S, Glassmeier K-H. On the excitation of ULF waves by solar wind pressure enhancements. Annales de Geophysique. 2006;**24**(11): 3161-3172

[19] Pilipenko V, Chugunova O, Engebretson M. Pc3–4 ULF waves at polar latitudes. Journal of Atmospheric and Solar-Terrestrial Physics. 2008; **70**(18):2262-2274

[20] Belakhovsky V, Pilipenko V, Murr D, Fedorov E, Kozlovsky A. Modulation of the ionosphere by Pc5 waves observed simultaneously by GPS/TEC and EISCAT. Earth, Planets and Space. 2016;**68**(1):1-13

[21] Balasis G, Papadimitriou C, Daglis IA, Pilipenko V. ULF wave power features in the topside ionosphere revealed by swarm observations. Geophysical Research Letters. 2015; **42**(17):6922-6930

[22] Regi M, De Lauretis M, Francia P. The occurrence of upstream waves in relation with the solar wind parameters: A statistical approach to estimate the size of the foreshock region. Planetary and Space Science. 2014;**90**:100-105

[23] De Lauretis M, Francia P, Regi M, Villante U, Piancatelli A. Pc3 pulsations in the polar cap and at low latitude. Journal of Geophysical Research: Space Physics. 2010;**115**(A11):A11223

[24] Lichtenberger J, Clilverd MA, Heilig B, et al. The plasmasphere during a space weather event: First results from the PLASMON project. Journal of Space Weather and Space Climate. 2013;**3**:A23

[25] Regi M, Francia P, De Lauretis M, Glassmeier KH, Villante U. Coherent transmission of upstream waves to polar latitudes through magnetotail lobes. Journal of Geophysical Research: Space Physics. 2013;**118**:6955-6963

[26] De Lauretis M, Regi M, Francia P, Marcucci MF, Amata E, Pallocchia G. Solar wind-driven Pc5 waves observed at a polar cap station and in the near cusp ionosphere. Journal of Geophysical Research: Space Physics. 2016;**121**(11): 11145-11156

[27] Glassmeier K-H, Motschmann U, Dunlop M, et al. Cluster as a wave telescope—First results from the fluxgate magnetometer. Annales de Geophysique. 2001;**19**(10/12): 1439-1447

[28] Clausen LBN, Yeoman TK, Fear RC, Behlke R, Lucek EA, Engebretson MJ. First simultaneous measurements of waves generated at the bow shock in the solar wind, the magnetosphere and on the ground. Annales Geophysicae. 2009; **27**:357-371

[29] Regi M, Del Corpo A, De Lauretis M. The use of the empirical mode decomposition for the identification of mean field aligned reference frames. Annals of Geophysics. 2016;**59**(6): G0651

[30] Francia P, De Lauretis M, Regi M. ULF fluctuations observed along the SEGMA array during very low solar wind density conditions. Planetary and Space Science. 2013;**81**:74-81

[31] Parkinson W. The influence of continents and oceans on geomagnetic variations. Geophysical Journal International. 1962;**6**(4):441-449

[32] Fujiwara S, Toh H. Geomagnetic transfer functions in Japan obtained by first order geomagnetic survey. Journal of Geomagnetism and Geoelectricity. 1996;**48**(8):1071-1101

[33] Regi M, De Lauretis M, Francia P, Lepidi S, Piancatelli A, Urbini S. The geomagnetic coast effect at two 80°S stations in Antarctica, observed in the ULF range. Annales de Geophysique. 2018;**36**(1):193-203

[34] Menk FW. Magnetospheric ULF waves: A review. In: The Dynamic Magnetosphere. Dordrecht: Springer; 2011. pp. 223-256

[35] Schulz M, Lanzerotti LJ. Particle diffusion in the radiation belts. Physics and Chemistry in Space. New York: Springer; 1974;**7**:215

[36] Elkington SR. A Review of ULF interactions with radiation belt electrons. In: Takahashi K, Chi PJ, Denton RE and Lysak RL editors. Magnetospheric ULF Waves: Synthesis and New Directions. American Geophysical Union; 2013. pp. 177-193. DOI: 10.1029/169GM12

[37] Elkington SR, Hudson MK, Wiltberger MJ, Lyon JG. MHD/particle simulations of radiation belt dynamics. Journal of Atmospheric and Solar-Terrestrial Physics. 2002;**64**: 607-615

[38] Engebretson M, Lessard M, Bortnik J, et al. Pc1–Pc2 waves and energetic particle precipitation during and after magnetic storms: Superposed epoch analysis and case studies. Journal of Geophysical Research: Space Physics. 2008;**113**(A1):A01211

[39] Mann IR, O'Brien TP, Milling DK. Correlations between ULF wave power, solar wind speed, and relativistic electron flux in the magnetosphere: Solar cycle dependence. Journal of Atmospheric and Solar-Terrestrial Physics. 2004;**66**(2):187-198

[40] Rodger CJ, Raita T, Clilverd MA, et al. Observations of relativistic electron precipitation from the radiation belts driven by EMIC waves. Geophysical Research Letters. 2008;**35** (16):L16106

[41] Blum LW, Halford A, Millan R, et al. Observations of coincident EMIC wave activity and duskside energetic electron precipitation on 18–19 January 2013. Geophysical Research Letters. 2015;**42**(14):5727-5735

[42] Regi M, De Lauretis M, Francia P. Pc5 geomagnetic fluctuations in response to solar wind excitation and their relationship with relativistic electron fluxes in the outer radiation belt. Earth, Planets and Space. 2015;**67**:9

[43] Arnoldy RL, Engebretson MJ, Denton RE, et al. Pc 1 waves and associated unstable distributions of magnetospheric protons observed during a solar wind pressure pulse. Journal of Geophysical Research: Space Physics. 2005;**110**(A7):A07229

[44] Regi M, Marzocchetti M, Francia P, De Lauretis M. A statistical analysis of Pc1–2 waves at a near-cusp station in Antarctica. Earth, Planets and Space. 2017;**69**(1):152

[45] Mursula K, Blomberg L, Lindqvist P-A, et al. Dispersive Pc1 bursts observed by Freja. Geophysical Research Letters. 1994;**21**(17):1851-1854

[46] Dyrud L, Engebretson M, Posch J, et al. Ground observations and possible source regions of two types of Pc 1-2 micropulsations at very high latitudes. Journal of Geophysical Research: Space Physics. 1997;**102** (A12):27011-27027

[47] Rodger CJ, Clilverd MA, Green JC, Lam MM. Use of POES SEM-2 observations to examine radiation belt dynamics and energetic electron precipitation into the atmosphere. Journal of Geophysical Research: Space Physics. 2010;**115**(A4):A04202

[48] Tinsley BA, Yu F. Atmospheric ionization and clouds as links between solar activity and climate. In: Pap JM, Fox P, Frohlich C, Hudson HS, Kuhn J, McCormack J, North G, Sprigg W and Wu ST editors. Solar Variability and Its Effects on Climate. American Geophysical Union (AGU); 2013. DOI: 10.1029/141GM22

[49] Tinsley BA, Heelis RA. Correlations of atmospheric dynamics with solar activity evidence for a connection via the solar wind, atmospheric electricity, and cloud microphysics. Journal of Geophysical Research: Atmospheres. 1993;**98**(D6):10375-10384

[50] Weimer D. Improved ionospheric electrodynamic models and application to calculating Joule heating rates. Journal of Geophysical Research: Space Physics. 2005;**110**(A5):A05306

[51] Weimer D. Predicting surface geomagnetic variations using ionospheric electrodynamic models. Journal of Geophysical Research: Space Physics. 2005;**110**(A12):A12307

[52] Yagova N, Lanzerotti L, Villante U, et al. ULF Pc5-6 magnetic activity in the polar cap as observed along a geomagnetic meridian in Antarctica. Journal of Geophysical Research: Space Physics. 2002;**107**(A8)

[53] Francia P, De Lauretis M, Vellante M, Villante U, Piancatelli A. ULF geomagnetic pulsations at different latitudes in Antarctica. Annales Geophysicae. 2009;**27**(9):3621-3629

[54] Regi M, De Lauretis M, Redaelli G, Francia P. ULF geomagnetic and polar cap potential signatures in the temperature and zonal wind reanalysis data in Antarctica. Journal of Geophysical Research: Space Physics. 2016;**121**(1):286-295

[55] Torrence C, Compo GP. A practical guide to wavelet analysis. Bulletin of the American Meteorological Society. 1998; **79**(1):61-78

[56] Grinsted A, Moore JC, Jevrejeva S. Application of the cross wavelet transform and wavelet coherence to geophysical time series. Nonlinear Processes in Geophysics. 2004;**11**(5/6): 561-566

[57] Regi M, Redaelli G, Francia P, De Lauretis M. ULF geomagnetic activity effects on tropospheric temperature, specific humidity, and cloud cover in Antarctica, during 2003–2010. Journal of Geophysical Research: Atmospheres. 2017;**122**:6488-6501

[58] Laken BA, Čalogović J. Composite analysis with Monte Carlo methods: An example with cosmic rays and clouds. Journal of Space Weather and Space Climate. 2013;**3**:A29

[59] Rosenfeld D, Lohmann U, Raga GB, et al. Flood or drought: How do aerosols affect precipitation? Science. 2008; **321**(5894):1309-1313

[60] Redaelli G, Lait R, Schoeberl M, et al. UARS MLS O3 soundings compared with lidar measurements using the conservative coordinates reconstruction technique. Geophysical Research Letters. 1994;**21**:1535-1538

[61] Payan S, Camy-Peyret C, Oelhaf H, et al. Validation of version-4.61 methane and nitrous oxide observed by MIPAS. Atmospheric Chemistry and Physics. 2009;**9**(2):413-442

[62] Yi W, Reid IM, Xue X, et al. First observation of mesosphere response to the solar wind high-speed streams. Journal of Geophysical Research: Space Physics. 2017;**122**(8):9080-9088

[63] Francia P, Regi M, De Lauretis M. Solar wind signatures throughout the high-latitude atmosphere. Journal of Geophysical Research: Space Physics. 2018;**123**:4517-4520. https://doi.org/ 10.1029/2018JA025411